UNIVERSITÀ DEGLI STUDI DI PADOVA

Dipartimento di Fisica e Astronomia "Galileo Galilei"

Corso di Laurea in Fisica

Tesi di Laurea

Dosimetric and radiobiological evaluation of Terbium radioisotopes

Relatore
Prof.ssa Laura De Nardo

Laureando
Elena Farinelli

Correlatore
Dott.ssa Laura Meléndez-Alafort

Anno Accademico 2021/2022

Contents

Introduction

During the twentieth century, Targeted Radionuclide Therapy (TRT) has emerged as an attractive tool for treating tumors. TRT is a treatment that uses radiopharmaceuticals to target and irradiate cancer cells. Radiopharmaceuticals (RP) contain a targeting molecule (e.g. peptide or antibody) linked to an appropriate radionuclide by a chelating agent; the targeting molecule binds to a tumor characteristic receptor by the lock and key principle.
TRT is based on the concept of delivering therapeutic doses of ionizing radiation to disease sites (usually metastases and disseminated tumor cells that can not be treated by the external beam radiation therapy, EBRT) in a way that causes minimal toxicity to the normal surrounding tissues.
Several are the advantages of this approach, namely, its selectiveness in radiating the target, relatively less severe and infrequent side effects, and the chance to evaluate the uptake by the tumor before therapy using nuclear medicine imaging techniques. The success of this treatment modality faces many challenges that include selection and availability of radionuclides with appropriate half-lives, emission characteristics, and availability of targeting vector capable of incorporating optimal radionuclide activity levels with favorable pharmacokinetics. Tumor response depends on tumor absorbed dose and tumor radiosensitivity. Some of the radiosotopes of the lanthanide series, such as Terbium and Lutetium, reveal suitable half-lives and distinct modes of decay schemes appropriate to nuclear medicine. While ^{177}Lu is being used in hospitals for therapy, current research on Terbium has been carried out and has been revealed as some of the most powerful tool for both therapy and diagnosis in the near future.
Terbium offers four radioisotopes ^{149}Tb, ^{152}Tb, ^{155}Tb, ^{161}Tb with complementary physical decay characteristics. These radioisotopes would allow the preparation of chemically-identical radiopharmaceuticals useful for PET (^{152}Tb) and SPECT diagnosis (^{155}Tb) and for α- (^{149}Tb) and β-particle (^{161}Tb) therapy. In this regard, Terbium radioisotopes are of particular interest and are compatible with the concept of theranostics in nuclear medicine.
"Theranostics" indicates the use of radiopharmaceuticals for diagnostic and therapeutic purposes. A way to apply theranostics is using a matched pair radioisotopes of the same element, one serving as a therapeutic agent and another aiding in diagnosis which allows to predict, prior to the treatment, the bio-distribution of the therapeutic radionuclide.
The knowledge of the radiopharmaceutical bio-distribution permits to estimate the dose received by the patient. Moreover, the treatment can be monitored especially when a single isotope emits both therapeutic particles and photons for imaging. Despite the members of the Terbium family represent a good option for theranostic pair, the use of this element for radionuclide therapy is not yet possible, because Terbium is an emerging radionuclide and radiopharmaceuticals labeled with their radioisotopes are not fully characterized.
The purpose of this work aims to investigate and compare the dosimetric and biological response to radiopharmaceuticals labeled with ^{149}Tb and ^{161}Tb radioisotopes. A software named MIRDcell will be utilized to calculate the cell absorbed dose in two lines of tumor cells and their response in terms of survival.

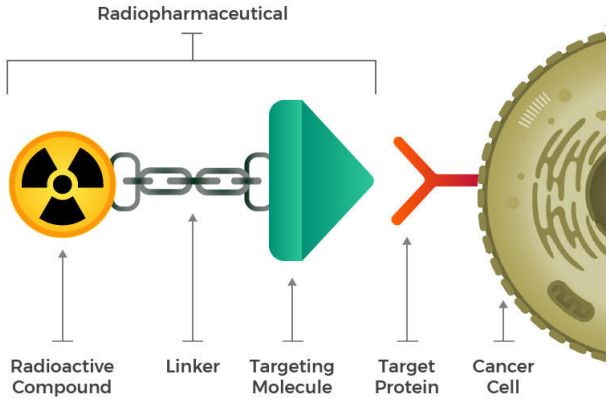

Figure 1: Radiopharmaceutical diagram (National Cancer Institute) [1]

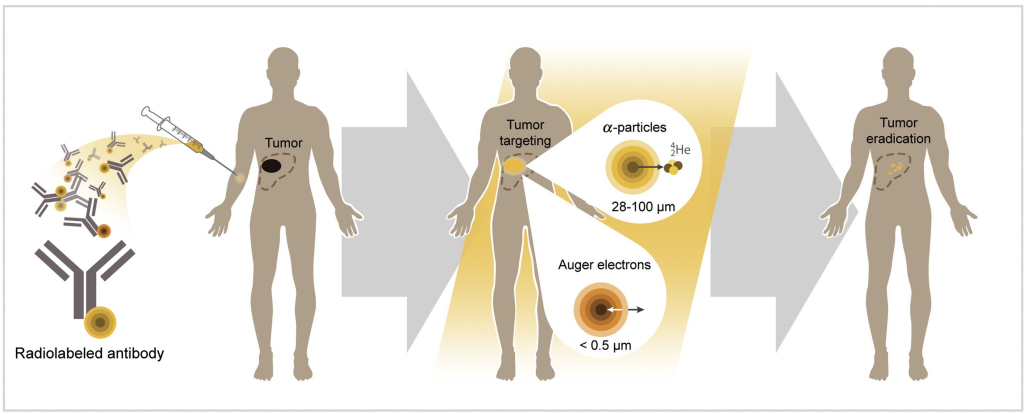

Figure 2: Aghevlian, Sadaf, Amanda J. Boyle, and Raymond M. Reilly. "Radioimmunotherapy of cancer with high linear energy transfer (LET) radiation delivered by radionuclides emitting α-particles or Auger electrons." Advanced drug delivery reviews 109 (2017): 102-118.

Chapter 1

Characteristics and production of Terbium radionuclides

In nuclear medicine, theranostics refers to the pairing of theraupetic-diagnostic radionuclides chelated to a biological vector. Therapy can be achieved with α, β or Auger and conversion electrons emitters, while radionuclides releasing γ rays or positron are useful for diagnosis.
The α-particles have high energy ($\sim$ 4–9 MeV), high linear energy transfer (LET $>$ 20 to hundreds of keV/μm), high relative biological effectiveness (RBE)[1] and low path range (40–100 μm, $\sim$ 1–3 cell diameter). Because their short range α particles are especially suitable for small tumors, isolated, or micro-clustered tumors.
β-particles have medium to high mean energy (0.5–2.3 MeV), low LET ($\sim$ 0.2 keV/μm) and a longer path-length (μm to few cm, $\sim$ 5–150 cell diameter), therefore, they may be suitable for large tumors or macro-clusters.
The Auger electrons have a very low-energy (eV-keV), a considerable LET (4–26 keV/μm) and because of their short path length of 2–500 nm their efficacy is limited to single cells, thus requiring the radionuclide to cross the cell surface and reach the nucleus range (few μm) with the help of an appropriate vector.
DNA is the principal target responsible for radiation-induced biologic effects such as cell killing, carcinogenesis and mutation. Different lesions (e.g., single-strand breaks (SSB), double-strand breaks (DSB), base damage, multiply damaged sites (MDS), DNA–protein cross-links) may be occurred by directly ionizing the DNA, or indirectly letting the free radicals interact with the DNA (mainly hydroxyl radicals deriving from water molecules that diffuse several nanometers). Most of these lesions are repaired readily except for DSB and MDS which cause critical DNA damage as well as cell death. The type of damage created and the distribution of ionization within DNA depend on incident particle and its energy. α particles are capable of creating a high-density linear tracks ionization and generating double-strand breaks that result in clusters of DNA damage. Because of their high LET and RBE, the damage is less reparable and the cells are inactivated by a few α particles. β particles generate infrequent ionizations along their path and are mainly responsible for single-strand breaks while Auger cascades, clusters of high ionization density causing DSB, but only if they are inside the cell nucleus and very close to the DNA molecule.

[1] The biological damage caused by ionizing radiations is expressed as the relative biological effectiveness (RBE), which it is defined as the ratio of the absorbed dose of a reference radiation (usually 250 keV of X-rays or γ rays emitted by ^{60}Co) to the dose of a radiation of interest to produce the same biological effects. Linear energy transfer (LET) is the average (radiation) energy deposited per unit path length along the track of an ionizing particle (keV/μm).

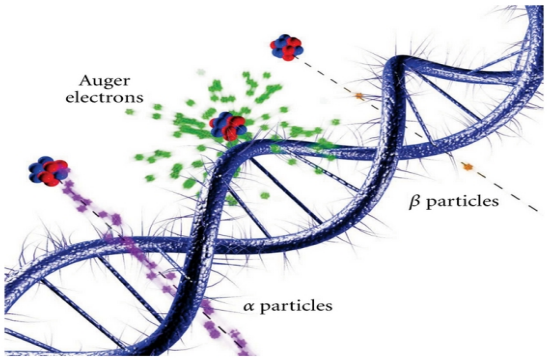

Figure 1.1: Interactions of ionizing radiations (Lee, Boon Q., et al. "Atomic radiations in the decay of medical radioisotopes: a physics perspective." Computational and mathematical methods in medicine 2012 (2012)).

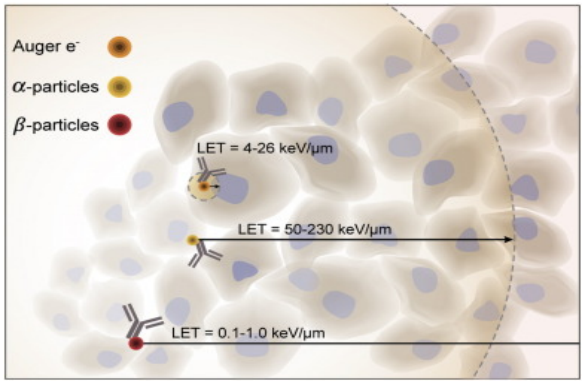

Figure 1.2: Illustration of the range of α, β particle and Auger electrons (Aghevlian, Sadaf, Boyle, Reilly. "Radioimmunotherapy of cancer with high linear energy transfer (LET) radiation delivered by radionuclides emitting α-particles or Auger electrons". Advanced drug delivery reviews 109 (2017): 102-118.)

The research on Terbium radionuclides has been performed after the initation in 2012 of the CERN MEDICIS (Medical Isotopes Collected from ISOLDE) project that aims to produce radionuclides for supplying hospitals. These four radioisotopes of Terbium ^{149}Tb, ^{152}Tb, ^{155}Tb, ^{161}Tb can provide suitable matched pairs for theranostic purpose and due to their identical chemical properties, formulation of RPs with identical pharmacokinetics for these species are easily possible. The primary proof-of-concept in favor of the unique quadruplet family was reported by Müller et al. [2] where the same targeting agent was used for in vivo experiments for different purposes.

Nuclide	Decay mode and branching	$T_{1/2}$	E_α (MeV)	$E_{\beta av}$ (MeV)	E_γ (keV)	I_γ (%)	Application
^{149}Tb	α (16.7%), β^+ (7.1%)	4.12 h	3.967	0.730	165.0	26	α-therapy
					352.2	29	
					388.6	18	
					652.1	16	
^{152}Tb	β^+ (17%)	17.5 h	—	1.080	271.1	8.6	PET
					344.3	65	
					586.3	9.4	
					778.9	5.8	
^{155}Tb	EC (100%)	5.32 d	—	—	86.55	32	SPECT
					105.3	25	
					180.1	7.5	
					262.3	5.3	
^{161}Tb	β^- (100%)	6.89 d	—	0.154	25.65	23	β^--/Auger therapy
					48.92	17	
					57.19	1.8	
					74.57	10	

Figure 1.3: Decay characteristics of Terbium radioisotopes [2]

1.1 ^{149}Tb

^{149}Tb is the only α-emitter radioisotope of Tb and with a suitable half-life (4.12 hours) for therapeutic applications among radiolanthanides. α-particles have a range of tissue penetration from 25 to 28μm with 3.967 MeV energy (intensity of 17%) and LET of 140–142 keV/μm. It can be labeled with peptides (small-molecular weight carriers) that are fast cleared from the body. ^{149}Tb emits both gamma rays (with an energy of 165 keV and intensity of 26.4 %), and β+ particle that help in its

detection through SPECT and PET imaging, respectively. ^{149}Tb has been proposed as a promising nuclide for targeted alpha therapy (TAT), however, there are many concerns about ^{149}Tb-TAT regarding its large-scale production and its long and complex decay chain (1.4). The daughter products are long-lived radionuclides, like ^{149}Gd (9.28 days), ^{145}Eu (5.39 d), ^{149}Eu (93.1 d), ^{145}Sm (340 d), and more. As reported by Beyer GJ et al. [3], it was supposed that by injecting the patient with 1 GBq ^{149}Tb-rituximab antibodies, after 1 year 100 kBq ^{149}Eu, 41 kBq ^{145}Sm, 2.2 kBq ^{145}Pm and after 10 years 50 Bq ^{145}Sm, 3.1 Bq ^{145}Pm, will remain in the patient's system. Therefor more trials are required to clarify any complication originating due to in vivo presence of these ^{149}Tb-decay products. One of the pre-clinical application of ^{149}Tb was reported by Beyer et al. [3]. The aim of that study was to demonstrate the effect of ^{149}Tb labeled with rituximab, a monoclonal antibody that targets CD20 (B-lymphocyte antigen expressed on the surface of all B-cells), on cancer cells in a severe combined immunodeficiency (SCID) mouse model of leukemia. It resulted that in 89% of treated mice any evidences of disease appeared for 4 months after a single injection of 5.5 MBq ^{149}Tb-labelled rituximab (5 μg per mouse), which corresponds to an injected dose of 280 MBq/kg body weight.
Another work was lead by Müller et al. [2] where ^{149}Tb labeled to DOTA-folate conjugate cm09 was injected in KB tumor-bearing mice. This proof-of-concept study demonstrated that tumor growth in mice that received targeted alpha therapy through ^{149}Tb-cm09 (2 injections of 1.1 and 1.3 MBq/-mouse) was constrained and, consequently, their survival time was significantly longer than that of untreated controls. Similarly, 2.2 MBq and 3.0 MBq per mouse of the same radioimmunoconjugate as above was administrated to KB tumor-bearing mice. An increasing survival time to 30.5 and 43 days, respectively, was observed in contrast to 21 days of untreated mice survival [4].
^{149}Tb is also positrons emitter and the potential of this radioisotope for PET/CT imaging was experimented for the first time in 2017 [4]. ^{149}Tb-DOTANOC (7 MBq) was injected in AR42J tumor-bearing mouse and 2 hours later PET/CT diagnosis provided high quality images of the tumor.

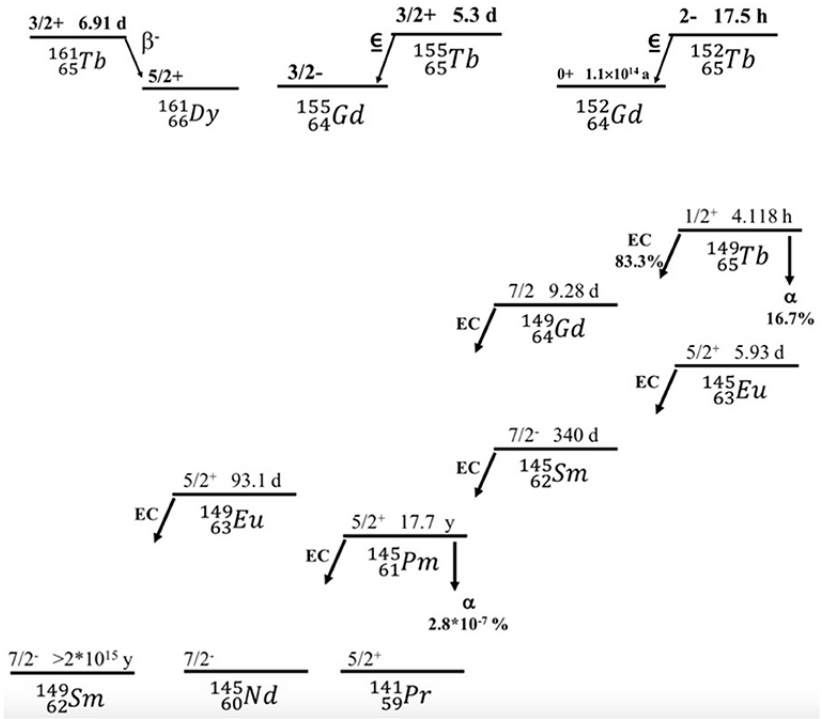

Figure 1.4: Decay chain of Terbium radioisotopes [1]

1.2 ^{152}Tb

^{152}Tb has a half-life of 17.5 hours, decays by realising $\beta+$ particles of an average energy of 1.080 MeV (intensity of 17%) and emits also γ rays (figure 1.3). It represents an interesting tool for diagnosis especially for PET and it could be suitable for dosimetry and monitoring ^{149}Tb bio-distribution in radiotherapy.
In 2012 Muller et al.[2] studied the potential of ^{152}Tb for PET imaging using a DOTA-folate conjugate (cm09), in KB tumor-bearing mice, injected after 14 days cancer cell inoculation. ^{152}Tb-cm09 provided great images of tumor xenografts of mice (figure 1.5).
In 2016 ^{152}Tb has been the first isotope tested in a male patient with diagnosed metastatic neuroendocrine neoplasm [4]. A 145 MBq of ^{152}Tb-DOTATOC was injected and PET/CT scans were performed over a period of 24 hours with results of even small metastases visualization. Due to its longer half-life than ^{68}Ga's (68 minutes), it was stated that ^{152}Tb would be preferable to evaluate dosimetry before radiotherapy [4].
Another study [4] using the somatostatin analog DOTANOC labeled to ^{152}Tb and administrated to a pancreatic tumor-bearing mouse, had shown from PET/CT scans the same tissue distribution of ^{177}Lu-DOTANOC's. In this regard ^{152}Tb could be used for imaging and dosimetry prior to the therapy with ^{177}Lu.

1.3 ^{155}Tb

^{155}Tb has a half-life of 5.32 days, decays by electron capture (EC) and emits γ radiations of 86.55 keV and 105.3 keV (figure 1.3) that make this radionuclide suited for low-dose SPECT imaging.
It may be of particular interest for visualizing and staging malignancies and calculating dosimetry prior to therapy with a therapeutic match such as the $\beta-$-emitting radiolanthanides ^{177}Lu and ^{161}Tb. Due to its γ rays, ^{155}Tb could also be applied in gamma camera scintigraphy.
^{155}Tb was performed through Derenzo phantom studies (a common quality control phantoms for nuclear medicine imaging)[4]. With SPECT/CT technique high quality images were obtained with an excellent spatial resolution compared to currently employed ^{111}In. An in vivo application of ^{155}Tb-cm09 allowed excellent tumor visualization of KB tumor-bearing mice via SPECT, at 24 h after injection (figure 1.5).

1.4 ^{161}Tb

^{161}Tb has a half life of 6.89 days and emits $\beta-$ -particles of an average energy of 0.154 MeV with an intensity of 100% as well as Auger and conversion electrons (about 12 e^-/decay with low energy $\sim$ keV), and γ radiation with different energies and intensity suitable for SPECT (figure 1.3). These low energy electrons have high LET which can be effective in decreasing the survival capacity of cancer cells.
The first preclinical study with ^{161}Tb was conducted in 1995 by De Jong et al. (as reported in [4]) where ^{161}Tb-octreotide was used to investigate the bio-distribution in normal mice. It resulted that ^{161}Tb-octreotide cleared faster from the blood than ^{111}In-octreotide, but it was absorbed faster in liver.
In 2012 Müller et al.[2] performed the first therapy application of ^{161}Tb, using DOTA–folate conjugate cm09 labeled with the radioisotope and injected 11 MBq in five KB tumor-bearing mice. Compared to other five untreated mice, tumor growth was reduced in 4 mice, and only 1 mouse had an attenuated growth. The average survival of control mice (not treated) was 28 days and they had to be euthanized, while 4 out of 5 treated ones were still alive at day 56. Only the treated mouse that did not experience tumor regression had to be euthanized because of its larger tumor at day 38.

A study conducted in [5] has identified ^{161}Tb as a better candidate than ^{177}Lu to irradiate single tumor cells and micrometastases in targeted radionuclide therapy. Regardless of the uptake of the radionuclide, in all regions of the cell (surface, cytoplasm, nucleus) the absorbed dose, calculated with Monte Carlo track-structure (MCTS) code CELLDOSE, delivered by ^{161}Tb was higher (e.g. 5 Gy to the nucleus from the radiopharmaceutical localized on the cell surface) than the dose delivered by ^{177}Lu (1.9 Gy). The absorbed dose of ^{161}Tb was also higher in cell clusters. This radiolanthanide has gained attention as an alternative to ^{177}Lu due to its medium-energy $\beta-$ -particles, similar to ^{177}Lu, in addition with Auger and conversion electrons which provide a higher localised dose. Therefore, ^{161}Tb may be a promising radionuclide for adjuvant therapy, such as TRT for residual tumor tissue, as well as for advanced disease therapy.
A further study that proves a better efficiency of ^{161}Tb over ^{177}Lu is reported by Müller et al. in [6]. ^{161}Tb-cm09 and ^{111}Lu-cm09 were investigated in two different tumor mouse models: KB (human cervical carcinoma) and IGROV-1 (human ovarian carcinoma) tumor xenografts. At the same activity (10 MBq, 0.5 nmol) ^{161}Tb-cm09 was more effective to reduce KB and IGROV-1 tumor growth than ^{177}Lu-cm09 due to its higher absorbed dose (3.3 Gy/MBq) compared to ^{177}Lu-cm09 (2.4 Gy/MBq). The median survival time in KB tumor-bearing mice was 31 days for control mice, 54 days for mice treated with ^{161}Tb-cm09 and 35 days for mice treated with ^{177}Lu-cm09. In those with IGROV-1 tumor xenografts the average survival time was 19 days for control mice, 31 and 30 days for mice treated with ^{161}Tb-cm09 and ^{177}Lu-cm09, respectively. In this study the potential of SPECT imaging was also investigated. It resulted that both radioconjugates gave excellent imaging quality.

1.5 Terbium production

1.5.1 ^{149}Tb, ^{152}Tb, ^{155}Tb production

^{149}Tb can be produced by direct and indirect nuclear reactions of charged particles (protons, α-particles, heavy ions) with the target material. Promising routes for direct reactions are ^{152}Gd (p,4n) nuclear reaction and spallation of tantalum foil target with high energy protons. However, irradiation of partial enrichment of ^{152}Gd targets (at present about a 30% level of enrichment is possible) inducing ^{152}Gd (p,4n)^{149}Tb reaction will be generating final product that would be contaminated by other terbium radioisotopes and rare earth isotopes. Moreover, ^{152}Gd is not currently available since its natural abundance is only 0.2%. As regard spallation reaction, ^{149}Tb, ^{152}Tb, ^{155}Tb were produced with success as reported by Müller et al.[2]. The spallation products were released from the tantalum foil, ionized, and mass separated according to their mass-to-charge ratio using the online isotope separator ISOLDE at CERN. Thus, the radioisotopes were collected on zinc-coated gold foil and after dissolution of the zinc layer in 0.1 M *HCl* they were separated from the zinc and isobar and pseudoisobar impurities through cation exchange chromatography and α-hydroxyisobutyric acid as an elution agent. The fractions of the radioisotopes in this acid solution were straightly combined with tumor-targeting ligands.
An indirect way to produce ^{149}Tb could be via the ^{142}Nd(^{12}C, 5n)^{149}Dy $\rightarrow$ ^{149}Tb or directly via the ^{141}Pr(^{12}C,4n)^{149}Tb, however, with lower production yields and radionuclidic purity compared to (p, 4n) reaction. In Dubna, Russia, 2.7 MBq of ^{149}Tb was produced at the heavy ion cyclotron from 1.25 hours irradiation of a 12 mg/cm^2 $^{nat}Nd_2O_3$ target with 108 MeV carbon ions. It was estimated that 15-30 GBq of ^{149}Tb could be obtained by irradiation of 60 mg/cm^2 ^{142}Nd target for 8-10 hours with 120 MeV ^{12}C ions [7].

As regards ^{152}Tb, in addition to high-energy proton-induced spallation of tantalum, its production at a cyclotron via the suitable ^{152}Gd(p,n)^{152}Tb nuclear reaction would be difficult because of the lack of this highly-enriched target material and the presence of other stable Gd isotopes in the target as well as the resulting terbium radioisotopes contamination.

Differently, highly-enriched ^{155}Gd target material is commercially available and, therefore, it could be used to produce relevant yields of ^{155}Tb via the ^{155}Gd(p,n)^{155}Tb reaction.
The indirect production route through ^{159}Tb(p,5n)^{155}Dy $\rightarrow$ ^{155}Tb can also provide high quantities of ^{155}Tb. The stable ^{159}Tb isotope makes this reaction in advantage but ^{155}Tb is not in a no-carrier-added state, on the contrary, it is always combined with bulk Terbium. Also, Dysprosium radioisotopes and their daughter products would contaminate the yield.

1.5.2 ^{161}Tb production

^{161}Tb is the only radioisotopes that can be produced in sufficient amounts. Its production was proposed by Lehenberger et al.[4] via the ^{160}Gd(n,γ)^{161}Gd $\rightarrow$ ^{161}Tb nuclear reaction, similar to ^{177}Lu's. Highly-enriched ^{160}Gd targets were irradiated for 2–3 weeks at the spallation-induced neutron source SINQ at Paul Scherrer Institute (PSI) or for 1 week at the high neutron flux nuclear reactor at Institut Laue-Langevin (ILL), France. Separation of ^{161}Tb from Gadolinium target was achieved at PSI by ion exchange chromatographic methods. In this way it was possible to provide the product in a solution of dilute *HCl*.

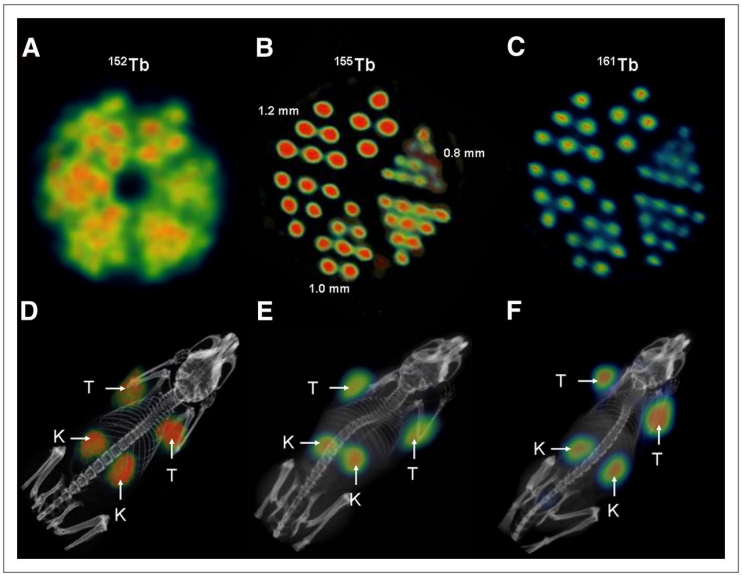

Figure 1.5: (A) PET image of Derenzo phantoms (∼1.9 MBq of ^{152}Tb). (B and C) SPECT images of Derenzo phantoms (∼0.6 MBq of ^{155}Tb and ∼50 MBq of ^{161}Tb, respectively). (D) PET/CT image of KB tumor–bearing mouse at 24 h after injection of ^{152}Tb-cm09, (E and F) SPECT/CT images of KB tumor–bearing mice at 24 h after injection of ^{155}Tb-cm09 (E) and ^{161}Tb-cm09.[2]

Chapter 2

MIRDcell software tool for multicellular dosimetry and bioeffect modeling

For this work an applet software application called MIRDcell V3 was used to compare the surviving fraction of cells treated with a radiopharmaceutical labeled with ^{149}Tb and ^{161}Tb radionuclides.
A Java applet was created by Rutgers University in association with the MIRD Committee of the Society of Nuclear Medicine and Molecular Imaging in order to ease multicellular dosimetry and biologic-response modeling.
MIRDcell models the distribution of radiopharmaceuticals within the different cell regions, estimates the absorbed dose, and predicts the surviving fraction of the labeled and unlabeled cell populations. Running the software, a graphical user interface consisting of a multitabbed panel is displayed.
First and foremost, the user selects the desired radionuclide from the tab named "Source Radiation" Three choices are available: predefined MIRD radionuclide, monoenergetic particle emitter, and user-defined radionuclide. The predefined MIRD radionuclide choice gives "β Full Energy Spectrum" and "β Average Energy Spectrum" options. The former provides a list of the radionuclides whose radiation data can be found in the MIRD monograph on radionuclide data and decay schemes. However, the yield and mean energies for all β- particle and positron emitters were replaced with full logarithmically binned β spectra. In cellular dosimetry, the continuous β spectrum is preferred to the mean β energy, however, the computation time is sensibly longer. The recoil energy of the residual daughter after a decay was not included in the calculation because experiments indicate that this energy is not biologically relevant. γ and X rays and neutrons were not also included since are not relevant for small size of cell. "β Average Energy Spectrum" option contains average β particles energies.
Upon the user selection of the desired radionuclide, into the box "Input Data for Calculation" are reported the name of the radionuclide, physical half-life, principal decay type, and radiation data. These include the total number of radiations in the file and the radiation type, yield, energy (MeV), and mean energy emitted per nuclear transition for each radiation Δ_i.
Cells are represented as two concentric spheres with a radius for the nucleus (RN) and for the cell (RC), and are considered as liquid water of unit density. The "Cell Source/Target" tab allows the user to select the source region such as cell (C), nucleus (N), cell surface (CS) and cytoplasm (Cy), where the radioactivity is localized, and the target regions C, N and Cy, for which the radiation absorbed dose is calculated and used for bio-effect modeling.
In Multicellular Geometry section there are three tabs: cell pair tab, 2-D colony and 3-D cluster. The first one illustrates the cell geometry that is used to calculate the self- and cross-doses for a pair

of cells and the distance between the centers of two cells is set by the user. Moreover the self-dose and cross-dose S coefficients, representing the mean absorbed dose per unit cumulated activity in the source region for the defined source and target regions, are calculated. Self-dose refers to the absorbed dose to cell compartments (C, N, Cy) from radiations emitted by decays within source regions of the same cell (C, N, Cy, CS). Cross-dose refers to absorbed dose to cell compartments from radiations emitted by decays in source regions of neighboring cells. The general formula for calculating the S coefficient to target region r_T from radiation type ICODE emitted by decays in source region r_S is given by

$$S_{ICODE}^{self/cross}(r_T \leftarrow r_S) = \sum_{irad=1}^{irad=N} \frac{\Delta_{ICODE,irad} \times \phi_{ICODE,irad}(r_T \leftarrow r_S)}{m(r_T)} \tag{2.1}$$

where $\Delta_{ICODE,irad}$ is the mean energy emitted per nuclear transition of the $irad^{th}$ radiation of type ICODE, $\phi_{ICODE,irad}$ is the fraction of energy emitted from the source region r_S that is absorbed in the target region r_T for the $irad^{th}$ radiation of type ICODE and m(r_T) is the mass of the target region r_T. The self-dose and cross-dose S coefficients are calculated using stopping powers and geometric factors. 2-D colony tab is used to create a cell population that stays on a plane (i.e. colony), whereas, the 3-D one generates it in the form of a multicellular cluster. In the Cell Geometry box, the user controls the packing density by adjusting the distance between cells (μm). The default packing arrangement is a close-packed cubic lattice (packing density 52 %) which indicates that there is no space between cells. The shape of the cluster can be changed among sphere, ellipsoid, rod, or cone. The desired dimensions of the cluster are then entered along with the time-integrated activity coefficient ($\tilde{a}$), mean activity per cell (labeled + unlabeled cells), and percentage of cells labeled. The time-integrated activity coefficient (unit of Bq h/Bq) represents the cumulative number of nuclear transformations $\tilde{A}(r_S, T_D)$ (Bq s) occurring in source tissue r_S over a dose-integration period T_D per unit administered activity A_0 (Bq). Furthermore, a Cold Region, where the radiopharmaceutical is restricted from specified regions of the cluster, can also be specified by setting the depth of penetration in the cluster.
Visual representations of the designated cell cluster, as well as its cross section, with color-coded labeled and unlabeled cells, along with shading indicating alive and dead cells are provided in the 3-D Cluster tab as in figure 2.1. Many plots can be visualized such as the survival curve for all the cells in the cluster, activity histogram, cumulative dose volume histogram and radial histogram (when the distribution of the activity is radially dependent).
To calculate the probability that a given cell survives, the applet uses a modified Linear Quadratic (LQ) model where the probability $P(r_k)$ that the k^{th} cell that receives an absorbed dose to target region r_k survives is calculated as follows:

$$P(r_k) = e^{-\alpha_{self}D_{self}-\beta_{self}D_{self}^2} e^{-\alpha_{cross}D_{cross}-\beta_{cross}D_{cross}^2} \tag{2.2}$$

where α_{self} and β_{self} identified the cellular response to self-dose (D_{self}), α_{cross} and β_{cross} characterize the cellular response to cross-dose (D_{cross}), and the effect of self and cross-dose are independent. This model assumes that each term is independent (non-interacting) and therefore different radiation types impart damage independent of one another. In addition, the self-dose imparts damage independent of the cross-dose and vice versa and the effect on one target (nucleus) is independent of the effect on another target (cytoplasm). The absorbed dose D to target region can be calculated as follows

$$D(r_T, T_D) = \sum_{r_s} f_{r_S} \tilde{A}(r_S, T_D) S(r_T \leftarrow r_S) \tag{2.3}$$

where $\tilde{A}(r_S, T_D)$ is the time-integrated activity (or total number of nuclear transformations) in source region over a period T_D and f_{r_s} is the fraction of cell activity in the source region. Labeled cells receive both self- and cross-doses, whereas unlabeled cells receive only cross-dose. In "Simple Radiobiological

Parameters" tab the user can specify α_{self}, β_{self}, α_{cross}, and β_{cross} parameters, while in "Complex Radiobiological Parameters" tab they can be specified not only for self-dose and cross-dose, but also independently for each type of radiation (α, β, Auger, etc.) and for each target region (C, N, Cy). In this case the probability that the kth cell survives is obtained by taking the product of the probabilities corresponding to each radiation type

$$P(r_T^k) = \prod_{ICODE=1}^{N} P_{ICODE}(r_T^k) \tag{2.4}$$

where

$$\begin{aligned} P_{ICODE}(r_T) = e^{-\alpha^{self}_{ICODE}(r_T \leftarrow r_S) D^{self}_{ICODE}(r_T \leftarrow r_S) - \beta^{self}_{ICODE}(r_T \leftarrow r_S)(D^{self}_{ICODE}(r_T \leftarrow r_S))^2} \\ \times e^{-\alpha^{cross}_{ICODE}(r_T \leftarrow r_S) D^{cross}_{ICODE}(r_T \leftarrow r_S) - \beta^{cross}_{ICODE}(r_T \leftarrow r_S)(D^{cross}_{ICODE}(r_T \leftarrow r_S))^2} \end{aligned} \tag{2.5}$$

The determination of whether a given cell survives or not is determined by a Monte Carlo method. Briefly, for each cell, a survival probability is calculated by the equation 2.2 or 2.4 depending on which radiobiological parameters are used. A random number between 0,0 and 1,0 is generated and compared with the survival probability. If the random number is smaller than the calculated probability, the cell is scored as a survivor and as dead otherwise. This process is then repeated for every cell in the population. The fraction of survivors among the cell population represents the surviving fraction of the cell population. This process is repeated for numerous values of the mean cell activity <A> up to a maximum value of mean activity per cell. The distribution of activity among the labeled cells is selected in the Cell Labeling box by the user. Three distribution options are available such as uniform, normal and lognormal distribution. All activity distributions undergo a normalization within MIRDcell to satisfy $<A> = \frac{1}{N}\sum_{i=1}^{N} A_i$ where N is the number of cells in the colony and A_i activity in the i^{th} cell. A uniform activity distribution implies that each labeled cell has the same initial activity A in its source region. In the normal and lognormal distribution, the initial activity per cell is distributed randomly among the labeled cells according to their probability density function.
There is also a Multi-Drug tab which enables the user to specify multiple drugs (radiopharmaceuticals) in a cluster of cells and then simulate the surviving fraction. Finally, in the output tab all the data calculated and used to create the plots are shown such as mean activity per cell (MAC), mean absorbed dose to target region(s) of cells (MDC), and more.

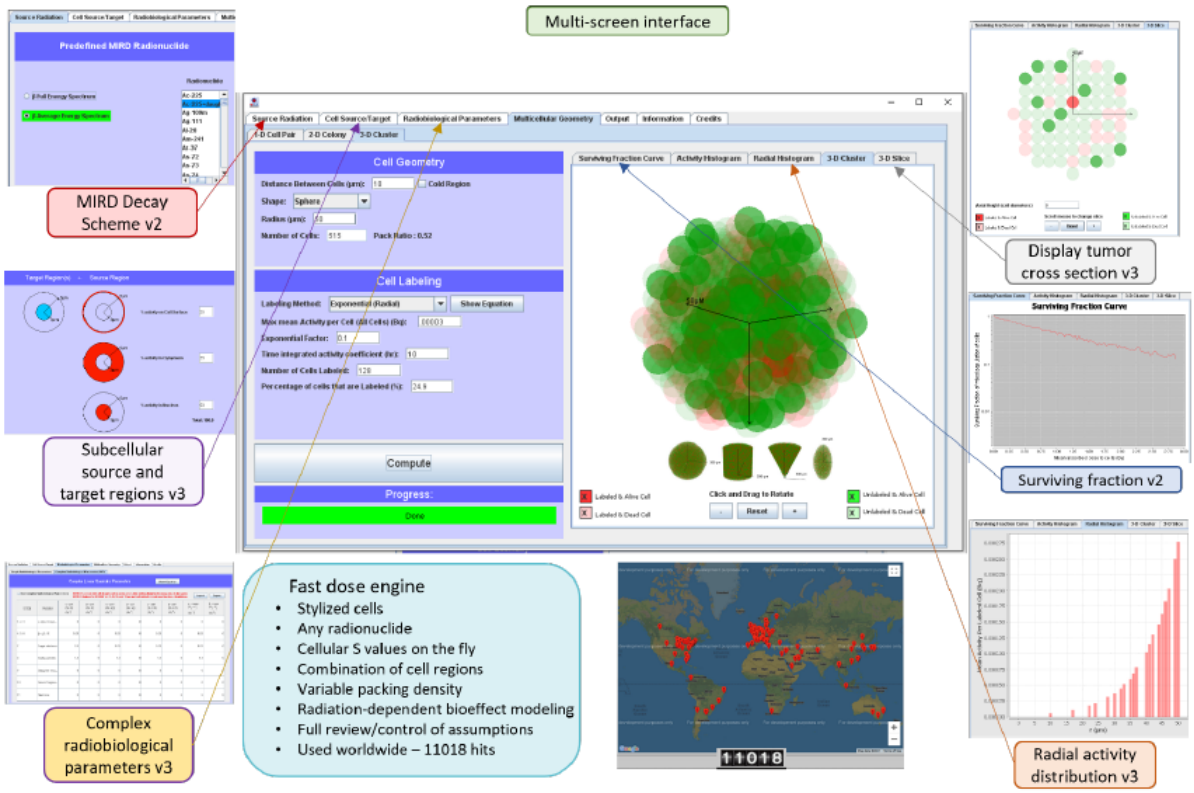

Figure 2.1: Katugampola, Sumudu, et al. "MIRD Pamphlet No. 27: MIRDcell V3, a revised software tool for multicellular dosimetry and bioeffect modeling." Journal of Nuclear Medicine (2022).

Chapter 3

Materials and methods

Calculations were performed using MIRDcell program and two files containing the radiation data of ^{149}Tb and ^{161}Tb were created and used clicking the option "User Created Radionuclide". Each file, as reported in the previous chapter, contains an integer code (ICODE) that identifies the radiation type, the absolute yield of the radiation (number per nuclear transformation), the unique or average energy of the radiation (MeV), and a two-character mnemonic denoting the radiation type. The file of ^{149}Tb contains also the radiations emitted by daughters, since for internal dosimetry all decay chain of the radionuclide (1.4) must be considered. Each yield of the radiations emitted by daughters were multiplied by the branching fraction of the respective chain. In particular, the yields of ^{149}Gd and of its daughter ^{149}Eu were multiplied by branching fraction of 0,833, while ^{145}Eu and all its daughters by 0,167. As regards ^{161}Tb file, it was created using the continuous spectrum of $\beta-$. All of this data were taken from the file .RAD and .BET of ICRP publications 107, the International Commission on Radiological Protection.
In this work, the radius of the cell and of its nucleus was set at 10μm and 4μm respectively and it was assumed that the radioactivity was uniformly distributed inside the source region and that the distance between centers of neighboring cells was 20μm (cells touching one another).
To estimate the survival it was considered a 3D multicellular cluster with a radius of 130μm, containing 1189 cells and it was assumed that different percentages of the cells were labeled with radioactivity, specifically 10%, 30%, 50% and 80%. The program causally selects labeled cells in the cluster. Cell activity varies from zero up to a maximum activity which was set at 0,01 Bq per cell. The time integrated activity coefficient, also termed as residence time, which represents the cumulative number of nuclear transformations (Bq s) occurring in source tissue over a dose-integration period per unit administered activity A_0 (Bq), was set at 50 hours for both radionuclides.
MIRDcell estimates the surviving fraction by using the linear quadratic model as in 2.2 which describes a survival probability of a cell after exposure to a single dose of radiation. α_{self}, β_{self} and α_{cross}, β_{cross} parameters describes the cell's radiosensitivity to doses (D_{self}) and (D_{cross}), respectively. α term reflects that the cell is killed from a single hit events that cause a lethal damage, while β parameter represents multiple hit and is related to repairable damage by the cell itself. In this work it was considered $\alpha_{self} = \alpha_{cross} = \alpha$ and $\beta_{self} = \beta_{cross} = \beta$ and the values used are reported in [8] and they are related to two types of prostate cancer cell lines with different radiosensitivity, the LNCaP where α = 1,081 Gy^{-1}, β = 0 Gy^{-2}, and PC3 where α = 0,551 Gy^{-1} and β = 0,021 Gy^{-2}.
For each cell lines, different types of treatment were studied: it was taken the whole cell as source region and as target region, and a more realistic approach where it was assumed that the cell nucleus was the target region and separately nucleus, cytoplasm and cell surface as source region. Moreover, the table 3.1 shows the different activity distributions in the source regions that are taken into account for other calculations, considering the nucleus as target region. The percentages of activity in the source

regions were obtained from experimental data from three different radiopharmaceuticals labeled with ^{161}Tb, reported by Borgna et al.[9] (see Table 3.1).

Radiopharmaceutical	% of activity distribution in source regions		
	Nucleus	Cytoplasm	Cell surface
1	1%	80%	19%
2	2%	7%	92%
3	6%	78%	16%

Table 3.1: Different activity distributions in source regions

Finally, for this last approach it was also evaluated the survival of cells using complex radiobiological parameters which are reported in table 3.2. The complex parameters depend on the radiation type and the source-target regions. The distinction between self-dose and cross-dose parameters is relevant for radionuclides that emit Auger electrons, and low energy β-particles, when they are incorporated close to the DNA in the cell nucleus. It has been demonstrated that electrons with low energy can be more radiotoxic than α particles when they are close to the DNA [10]. Consequently, a high α-self value was used for AE and IE with energy lower than 40 KeV when the source region was the cell nucleus. The used α-self values of α-particles for this approach, were obtained from the values calculated by Tracy et al., after a cell treatment with α-particles of the same energy [11].

	LNCaP cell line			PC3 cell line		
Radiation	β-, β+, IE	Auger electrons	α particles	β-, β+, IE	Auger electrons	α particles
α-self (Gy^{-1}) n$\leftarrow$ n	1,081	2,3	1,4	0,551	2,3	1,4
β-self (Gy^{-2}) n$\leftarrow$ n	0	0	0	0,021	0	0
α-self (Gy^{-1}) n$\leftarrow$ cy	1,081	1,081	1,4	0,551	0,551	1,4
β-self (Gy^{-2}) n$\leftarrow$ cy	0	0	0	0,021	0,021	0
α-self (Gy^{-1}) n$\leftarrow$ cs	1,081	1,081	1,4	0,551	0,551	1,4
β-self (Gy^{-2}) n$\leftarrow$ cs	0	0	0	0,021	0,021	0
α-cross (Gy^{-1}) $n_i \leftarrow c_j$	1,081	1,081	1,4	0,551	0,551	1,4
β-cross (Gy^{-2}) $n_i \leftarrow c_j$	0	0	0	0,021	0,021	0

Table 3.2: Complex radiobiological parameters

Chapter 4

Results and discussion

4.1 Radionuclide 100% activity distribution in source regions

Table 4.1 shows S-values (mean absorbed dose per unit cumulated activity in the source region) for self-irradiation and for cross-irradiation from couple of cells at 20μm distance, calculated for ^{149}Tb and ^{161}Tb for different source-target configurations (target←source), assuming that the radionuclides were uniformly distributed in the source regions. For both radionuclides, the self-dose is the lowest for nucleus←cell surface configuration while it is the highest for nucleus←nucleus configuration. Cross-dose values become more similar for different configurations and this trend is increasing for increasing distance between the cells. Self-dose and cross-dose of ^{149}Tb are higher than those for ^{161}Tb, as expected, due to the higher energy emitted per decay by ^{149}Tb (0,6627MeV/nt of α particles and 0,0871 MeV/nt of electrons) and its daughter products compared to ^{161}Tb which is 0,2025 MeV/nt in the form of electrons.

^{149}Tb	cell← cell	nucleus← cell surface	nucleus← cytoplasm	nucleus← nucleus
Self-dose (Gy/Bq s)	6,92E-03	2,99E-03	5,93E-03	4,82E-02
Cross-dose (Gy/Bq s)	9,33E-04	8,88E-04	9,41E-04	1,08E-03
^{161}Tb				
Self-dose (Gy/Bq s	8,89E-04	2,02E-04	5,87E-04	8,56E-03
Cross-dose (Gy/Bq s)	4,84E-05	4,53E-05	4,19E-05	3,73E-05

Table 4.1: S-values for self-dose and cross-dose (Gy/Bq s) of ^{149}Tb and ^{161}Tb

For the cluster of cells, the mean absorbed dose to all cells increases linearly with the mean number of disintegrations per cell (for all cells), while the mean absorbed dose to labeled cells increases linearly with the mean number of disintegrations per labeled cell. The linear coefficients of these straight lines are reported in table 4.2 for the different source-target configurations and the different % of labeled cells. The mean number of decays per cell (labeled) is obtained as the product of the time integrated activity coefficient and the mean activity per cell (labeled). Mean absorbed doses calculated for LNCaP and PC3 cell lines are the same since it is considered the same cell model as well as S-values. For each source-target configuration, the linear coefficient of the mean absorbed dose to all cells is independent of % of labeled cells, while those of the mean absorbed dose to labeled cells increase with the % of labeling due to the effect of cross irradiation. For 10% of labeled cells values are only slightly higher than those reported in table 4.1 for self irradiation, but they increase linearly with % of labeled cells.

Mean absorbed dose/decay (all cells)					Mean absorbed dose/decay (labeled cells)				
^{149}Tb	**10%**	**30%**	**50%**	**80%**	**^{149}Tb**	**10%**	**30%**	**50%**	**80%**
cell← cell	1,51E-02	1,53E-02	1,53E-02	1,53E-02	cell← cell	7,78E-03	9,36E-03	1,12E-02	1,35E-02
nucleus← cell surface	1,13E-02	1,10E-02	1,13E-02	1,13E-02	nucleus← cell surface	3,83E-03	5,39E-03	7,18E-03	9,58E-03
nucleus← cytoplasm	1,41E-02	1,40E-02	1,40E-02	1,39E-02	nucleus← cytoplasm	6,70E-03	8,44E-03	1,00E-02	1,22E-02
nucleus← nucleus	5,57E-02	5,55E-02	5,56E-02	5,56E-02	nucleus← nucleus	4,89E-02	5,02E-02	5,18E-02	5,40E-02
^{161}Tb	**10%**	**30%**	**50%**	**80%**	**^{161}Tb**	**10%**	**30%**	**50%**	**80%**
cell← cell	1,90E-03	1,90E-03	1,90E-03	1,90E-03	cell← cell	9,81E-04	1,18E-03	1,37E-03	1,67E-03
nucleus← cell surface	1,20E-03	1,20E-03	1,20E-03	1,20E-03	nucleus← cell surface	2,96E-04	4,84E-04	6,87E-04	9,68E-04
nucleus← cytoplasm	1,50E-03	1,50E-03	1,50E-035	1,50E-03	nucleus← cytoplasm	7,00E-04	9,00E-04	1,00E-03	1,10E-03
nucleus← nucleus	9,50E-03	9,50E-03	9,50E-03	9,50E-03	nucleus← nucleus	8,60E-03	8,80E-03	9,00E-03	9,30E-03

Table 4.2: Linear coefficients (Gy/Bq s) of mean absorbed dose/decay (all cells) and mean absorbed dose/decay (labeled cells)

In figures 4.1 and 4.2 is plotted the surviving fraction of ^{149}Tb and ^{161}Tb for LNCaP and PC3 cell line respectively, as a function of the number of disintegrations per cell (all cells), considering cell←cell configuration and different percentages of labeled cells. When the percentage of labeled cells increases, the survival capacity of cells decreases. Because of higher cytotoxicity and higher ionization per unit range of α particle compared to β particle, ^{149}Tb provides a lower probability for cells to survive. In cell←cell configuration the surviving fraction of LNCaP cells treated with ^{149}Tb is about 1% with 400 disintegrations per cell when 80% of cells are labeled, while with ^{161}Tb the survival is less than 10% with more than 1200 disintegrations. Therefore, a large number of disintegrations are required to obtain the same level of survival. Surviving fraction of the less radiosensitive PC3 cell line is in general higher than LNCaP line due to its higher radioresistance.

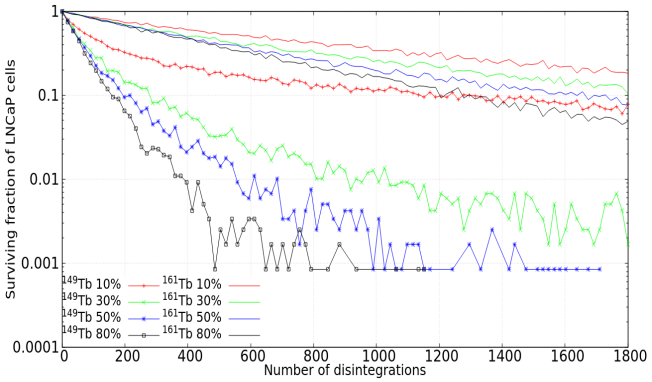

Figure 4.1: Surviving fraction of cell←cell configuration, LNCaP cell line

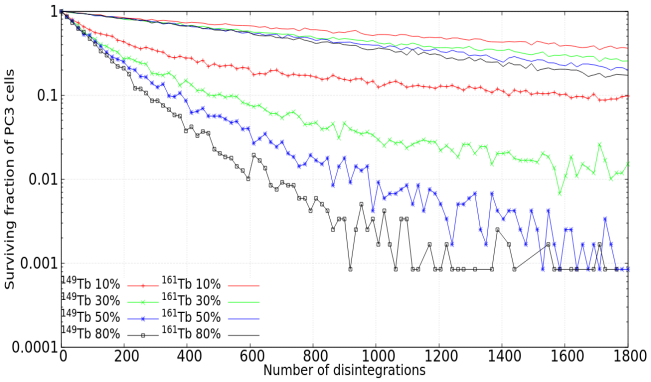

Figure 4.2: Surviving fraction of cell←cell configuration, PC3 cell line

The figures 4.3, 4.4 show a comparison between the surviving fraction of LNCaP and PC3 cells treated with ^{149}Tb and those with ^{161}Tb, as a function of the number of disintegrations per cell (all cells) for the different source-target configurations and for 50% of labeled cells. The survival, for LNCaP cell line treated with ^{149}Tb, is very similar regardless the different target←source configuration, except for nucleus←nucleus. For ^{161}Tb the survival is initially lower with nucleus←nucleus configuration, however, by increasing the number of disintegrations, the same level expected with cell←cell configuration is reached. The survival of PC3 cell line is higher than LNCaP cell line, but also in this case, a similar level of survival was achieved for high number of disintegrations regardless the specific localization of the radionuclide.

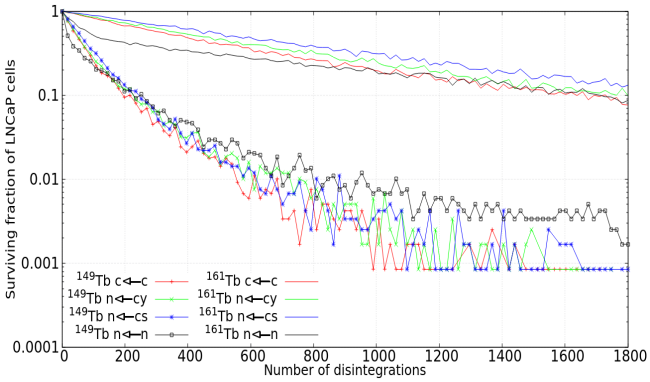

Figure 4.3: Surviving fraction of 50% of labeled cells with ^{149}Tb and ^{161}Tb, LNCaP line cell

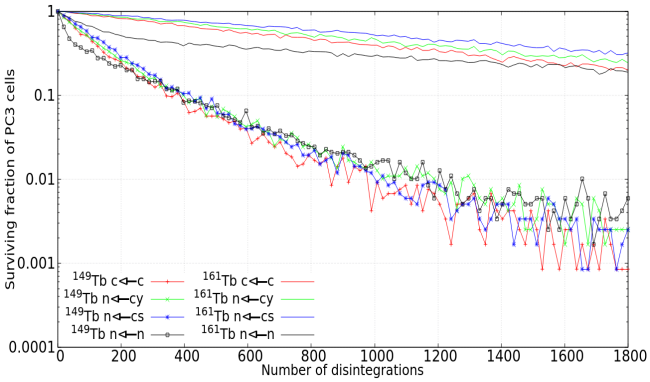

Figure 4.4: Surviving fraction of 50% of labeled cells with ^{149}Tb and ^{161}Tb, PC3 line cell

In figures 4.5, 4.6, 4.7 and 4.8 is plotted the surviving fraction of all cells as a function of the mean absorbed dose to all cells for LNCaP and PC3 cell lines, and ^{149}Tb and ^{161}Tb radionuclides, respectively. At low doses for both cell lines and radionuclides, the curves are quite similar for different source-target configurations but, by increasing the mean dose, nucleus← nucleus configuration evidences a higher survival. In this situation the dose imparted to the target is very high but, as the effect of cross irradiation is limited, only the labeled cells are irradiated and on the whole the survival is higher. By comparing the two cell lines, for both radionuclides to reach the same level of survival more dose is required in the case of PC3 cell line compared to LNCaP one.

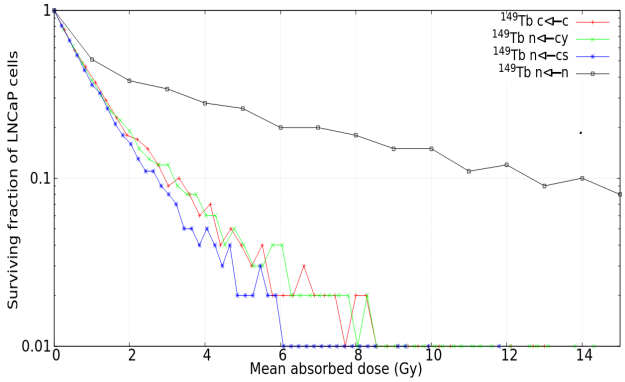

Figure 4.5: Surviving fraction of 50% of labeled cells with ^{149}Tb, LNCaP line cell

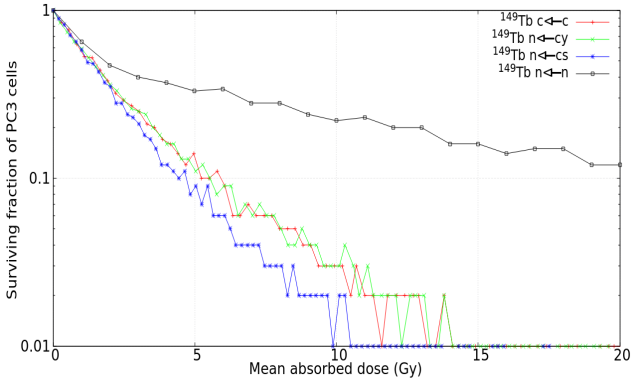

Figure 4.6: Surviving fraction of 50% of labeled cells with ^{149}Tb, PC3 line cell

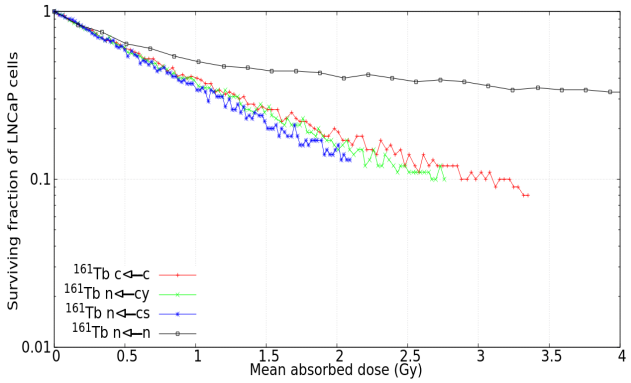

Figure 4.7: Surviving fraction of 50% of labeled cells with ^{161}Tb, LNCaP line cell

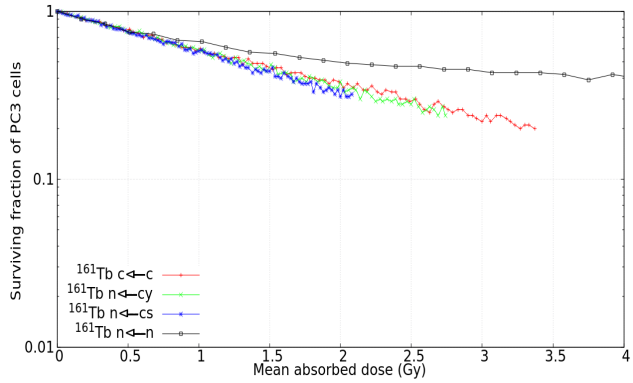

Figure 4.8: Surviving fraction of 50% of labeled cells with ^{161}Tb, PC3 line cell

4.2 Different percentages of radionuclide activity distribution in source regions

In table 4.3 are reported the S-values calculated for self-irradiation and for cross-irradiation from couple of cells at 20μm distance, for ^{149}Tb and ^{161}Tb considering the three different radiopharmaceuticals (RP) and assuming that the radionuclides were uniformly distributed in the source regions (see table 3.1). Self-dose and cross-dose of ^{149}Tb are higher than those for ^{161}Tb due to the higher energy emitted per decay by ^{149}Tb and its daughter products compared to ^{161}Tb. For both radionuclides, self-dose is higher when considering the configuration RP3, with 6% of the radionuclide in the nucleus and smaller for RP2, with the higher concentration on the cell surface. The contribution of self-dose increases when the target← source distance decreases, while the cross-dose decreases by rising that distance.

^{149}Tb	RP1	RP2	RP3
Self-dose (Gy/Bq) s	5,80E-03	4,13E-03	8,00E-03
Cross-dose (Gy/Bq s)	9,32E-04	9,04E-04	9,41E-04
^{161}Tb			
Self-dose (Gy/Bq s)	5,94E-04	3,99E-04	1,01E-03
Cross-dose (Gy/Bq s)	4,25E-05	4,53E-05	4,22E-05

Table 4.3: S-values for self-dose and cross-dose (Gy/Bq s) of ^{161}Tb and ^{161}Tb, different percentages of source regions.

For the cluster of cells, the linear coefficients of the mean absorbed dose to all cells as a function of the mean number of disintegrations for all cells, and of the mean absorbed dose to labeled cells as a function of the mean number of disintegrations for labeled cells, are reported in table 4.4 for the different RPs and the different % of labeled cells. Mean absorbed doses calculated for LNCaP and PC3 cell lines are the same since it is considered the same cell model as well as S-values. For both radionuclides, the linear coefficients of the mean absorbed dose to all cells of RP3 are higher than those of other RPs. The contribution of self-doses increases when the target← source distance decreases. The linear coefficients of the mean absorbed dose to labeled cells of the three different RPs show greater differences from one another and, especially, those of RP3 are higher due to a lower percentage of radionuclides activity on the cell surface compared to the others.

Mean absorbed dose/decay (all cells)					Mean absorbed dose/decay (labeled cells)				
^{149}Tb	**10%**	**30%**	**50%**	**80%**	**^{149}Tb**	**10%**	**30%**	**50%**	**80%**
RP1	1,39E-02	1,38E-02	1,38E-02	1,39E-02	RP1	6,40E-03	8,10E-03	9,90E-03	1,23E-02
RP2	1,22E-02	1,24E-02	1,25E-02	1,24E-02	RP2	4,90E-03	6,50E-03	8,30E-03	1,07E-02
RP3	1,60E-02	1,61E-02	1,61E-02	1,60E-02	RP3	8,80E-03	1,04E-02	1,21E-02	1,44E-02
^{161}Tb	**10%**	**30%**	**50%**	**80%**	**^{161}Tb**	**10%**	**30%**	**50%**	**80%**
RP1	1,50E-03	1,50E-03	1,50E-03	1,50E-03	RP1	7,00E-04	9,00E-04	1,10E-03	1,30E-03
RP2	1,40E-03	1,40E-03	1,40E-03	1,40E-03	RP2	5,00E-04	7,00E-04	9,00E-04	1,20E-03
RP3	2,00E-03	2,00E-03	2,00E-03	2,00E-03	RP3	1,10E-03	1,30E-03	1,50E-03	1,80E-03

Table 4.4: Linear coefficients (Gy/Bq s) of mean absorbed dose/decay (all cells) and mean absorbed dose/decay (labeled cells)

The figures 4.9 and 4.10 show the surviving fraction of LNCaP and PC3 cell line treated with ^{149}Tb and with ^{161}Tb, as a function of the number of disintegrations per cell (all cells), considering the radiopharmaceutical RP3 and different percentages of labeled cells.

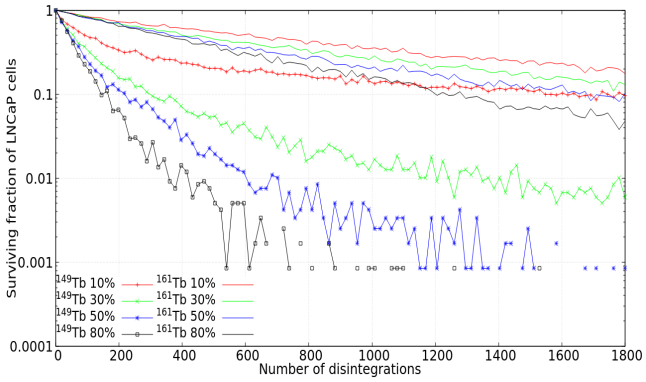

Figure 4.9: Surviving fraction of LNCaP cells treated with RP3

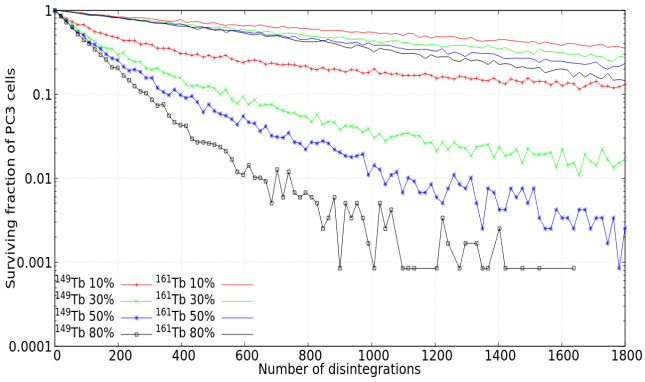

Figure 4.10: Surviving fraction of PC3 cells treated with RP3

As expected, when the percentage of labeled cells increases, the survival capacity of cells decreases. ^{149}Tb provides a lower probability for cells to survive. Because of the less radiosensitivity of PC3 cell line, the survival is in general higher than LNCaP cell line.
In figures 4.11 and 4.12 is plotted a comparison between the surviving fraction of LNCaP and PC3 cells respectively, treated with ^{149}Tb and those with ^{161}Tb, as a function of the number of disintegrations per cell (all cells) for different RPs and for 50% of labeled cells.
With 50% of labeled cells, a similar level of survival, for both cell line, is achieved regardless the different radiopharmaceutical (RP) used.

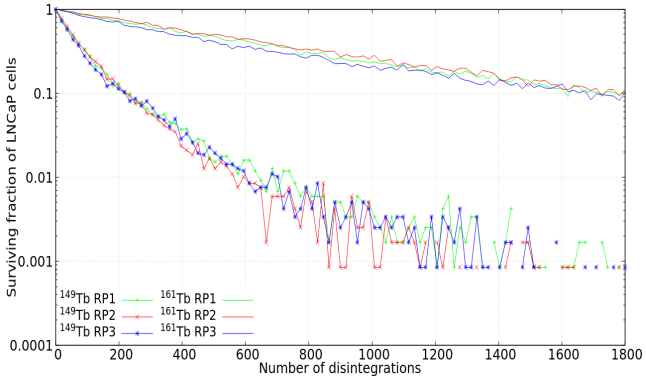

Figure 4.11: Surviving fraction of 50% of labeled cells with ^{149}Tb and ^{161}Tb, LNCaP line cell

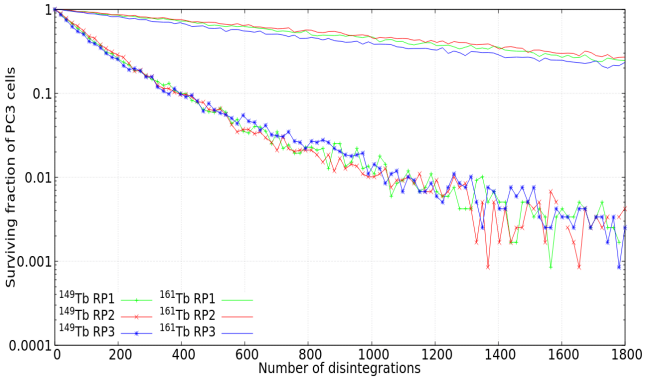

Figure 4.12: Surviving fraction of 50% of labeled cells with ^{149}Tb and ^{161}Tb, PC3 line cell

4.2.1 Analysis with complex radiobiological parameters

In the following calculations, the complex radiobiological parameters reported in table 3.2 were used only for radiopharmaceuticals RP1, RP2, and RP3.
S-values and mean absorbed doses for LNCaP and PC3 cell lines are the same as those in tables 4.2 and 4.4, respectively. Comparisons between the survival of both cell line treated with ^{149}Tb and ^{161}Tb using the simple linear quadratic model parameters and the survival of the cells using the complex radiobiological parameters (see table 3.2) are shown in figures 4.13, 4.14, 4.15 and 4.16.

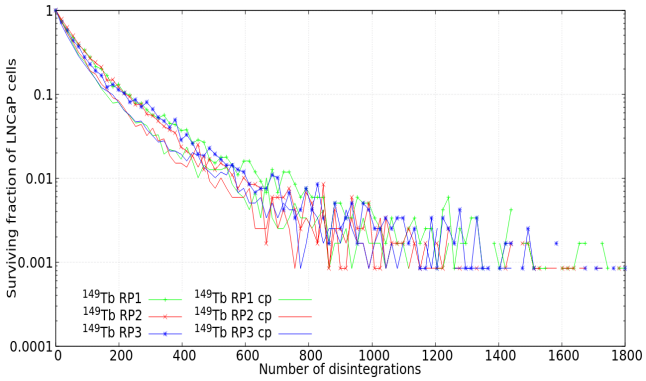

Figure 4.13: Comparison between the surviving fraction of 50% of labeled cells with ^{149}Tb using simple parameters and complex ones (cp), LNCaP cell line

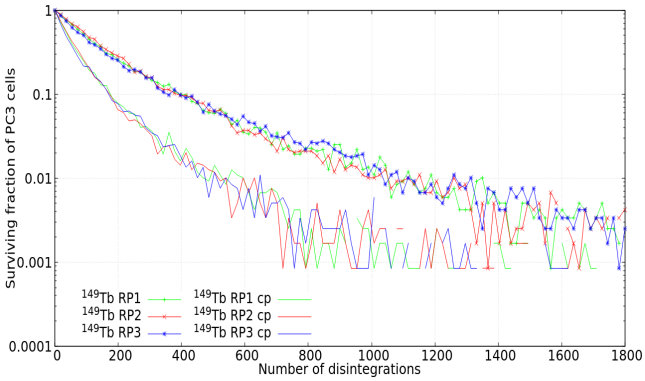

Figure 4.14: Comparison between the surviving fraction of 50% of labeled cells with ^{149}Tb using simple parameters and complex ones (cp), PC3 cell line

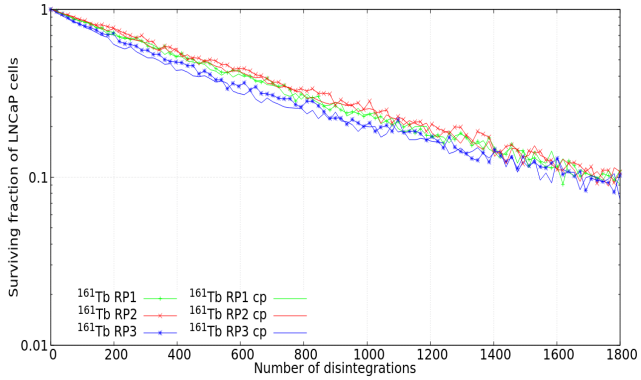

Figure 4.15: Comparison between the surviving fraction of 50% of labeled cells with ^{161}Tb using simple parameters and complex ones (cp), LNCaP cell line

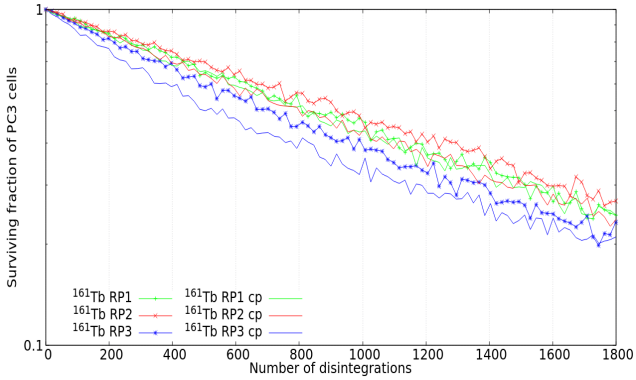

Figure 4.16: Comparison between the surviving fraction of 50% of labeled cells with ^{161}Tb using simple parameters and complex ones (cp), PC3 cell line

There are relevant differences between the surviving fractions after a treatment with ^{149}Tb using simple parameters and complex ones for PC3 cell line, due to an higher value of α_{self} and α_{cross} parameters for α particle (from 0,551 Gy^{-1} to 1,4 Gy^{-1}), for all RPs, and slight differences for the LNCaP cell line where the increase of this parameters is smaller (from 1,081 Gy^{-1} to 1,4 Gy^{-1}). No significant differences are found after a treatment with ^{161}Tb for LNCaP cell line, while for the PC3 cell line, there is a slight difference between RP3 with simple parameters and RP3 with complex ones. In this case, only α_{self} corresponding to Auger electron, in nucleus←nucleus configuration, is increased (from 0,551 Gy^{-1} to 2,3 Gy^{-1}), and therefore, there's a greater contribution when the percentage of ^{161}Tb activity in the nucleus is higher (6%), corresponding to RP3.

Chapter 5

Conclusions

The results derived from MIRDcell software, considering a rather unrealistic approach with 100% of activity in different cell source regions, show that there are differences in terms of cell survival. Conversely, with a more realistic approach based on experimental evidences, involving the three different radiopharmaceuticals, there are no relevant differences in terms of survival. In this case however, the use of complex radiobiological parameters instead of the simple ones changes the surviving fractions. Therefore, in order to evaluate real biological damage, it is important to know the localization of the radiopharmaceutical in the cell so that the appropriate radiobiological parameter, depending on the source-target arrangement and the radiation type, can be specified.
At parity of number of decays, the mean absorbed dose to all cells of ^{149}Tb is greater than ^{161}Tb. It is important to highlight how for calculations performed in this thesis, all ^{149}Tb decay chain is considered, consequently, the absorbed dose and the biological damage could be overestimated. The mean absorbed dose to cells in nucleus← nucleus configuration is the greatest, for this reason a lower survival should be expected. However, these higher values of doses provide a cell killing limited to labeled cells, while the neighboring unlabeled cells only receive a limited cross irradiation that is unable to kill them. Thus, the result is that only a few cells are killed. In this regard, the mean absorbed dose is not sufficient to predict the survival and what matters is the distribution of labeled cells in the cluster and the localization of the radiopharmaceutical within the different cell compartments.

Bibliography

[1] Nabanita Naskar and Susanta Lahiri. "Theranostic terbium radioisotopes: challenges in production for clinical application". In: *Frontiers in Medicine* 8 (2021).

[2] Cristina Müller et al. "A unique matched quadruplet of terbium radioisotopes for PET and SPECT and for α-and β–radionuclide therapy: an in vivo proof-of-concept study with a new receptor-targeted folate derivative". In: *Journal of nuclear medicine* 53.12 (2012), pp. 1951–1959.

[3] G-J Beyer et al. "Targeted alpha therapy in vivo: direct evidence for single cancer cell kill using 149Tb-rituximab". In: *European journal of nuclear medicine and molecular imaging* 31.4 (2004), pp. 547–554.

[4] Cristina Müller et al. "Scandium and terbium radionuclides for radiotheranostics: current state of development towards clinical application". In: *The British journal of radiology* 91.1091 (2018), p. 20180074.

[5] Mario E Alcocer-Ávila et al. "Radiation doses from 161Tb and 177Lu in single tumour cells and micrometastases". In: *EJNMMI physics* 7.1 (2020), pp. 1–9.

[6] Cristina Müller et al. "Direct in vitro and in vivo comparison of 161Tb and 177Lu using a tumour-targeting folate conjugate". In: *European journal of nuclear medicine and molecular imaging* 41.3 (2014), pp. 476–485.

[7] SN Dmitriev et al. "Lanthanides in nuclear medicine: preparation of 149Tb by irradiation with heavy ions". In: *Radiochemistry* 44.2 (2002), pp. 171–173.

[8] Ryo Saga et al. "Analysis of the high-dose-range radioresistance of prostate cancer cells, including cancer stem cells, based on a stochastic model". In: *Journal of radiation research* 60.3 (2019), pp. 298–307.

[9] Francesca Borgna et al. "Combination of terbium-161 with somatostatin receptor antagonists—a potential paradigm shift for the treatment of neuroendocrine neoplasms". In: *European journal of nuclear medicine and molecular imaging* (2021), pp. 1–14.

[10] Roger W Howell et al. "The question of relative biological effectiveness and quality factor for Auger emitters incorporated into proliferating mammalian cells". In: *Radiation research* 128.3 (1991), pp. 282–292.

[11] Bliss L Tracy et al. "Variation in RBE for survival of V79-4 cells as a function of alpha-particle (helium ion) energy". In: *Radiation research* 184.1 (2015), pp. 33–45.

[12] Amin I Kassis. "Therapeutic radionuclides: biophysical and radiobiologic principles". In: *Seminars in nuclear medicine*. Vol. 38. 5. Elsevier. 2008, pp. 358–366.

[13] Behrooz Vaziri et al. "MIRD pamphlet no. 25: MIRDcell V2. 0 software tool for dosimetric analysis of biologic response of multicellular populations". In: *Journal of Nuclear Medicine* 55.9 (2014), pp. 1557–1564.

[14] Sumudu Katugampola et al. "MIRD Pamphlet No. 27: MIRDcell V3, a revised software tool for multicellular dosimetry and bioeffect modeling". In: *Journal of Nuclear Medicine* (2022).

[15] S Murty Goddu, Dandamudi V Rao, and Roger W Howell. "Multicellular dosimetry for micrometastases: dependence of self-dose versus cross-dose to cell nuclei on type and energy of radiation and subcellular distribution of radionuclides". In: *Journal of Nuclear Medicine* 35.3 (1994), pp. 521–530.

[16] Wesley E Bolch et al. "MIRD pamphlet no. 21: a generalized schema for radiopharmaceutical dosimetry—standardization of nomenclature". In: *Journal of Nuclear Medicine* 50.3 (2009), pp. 477–484.